Numerical Analysis of Unsteady Transonic Flow over Rocket Nose

SOMDEB BANDOPADHYAY
School of Mechanical and Aerospace Engineering
Gyeongsang National University
sb020287@gmail.com
DONG-HYUN KIM
School of Mechanical and Aerospace Engineering
Gyeongsang National University
dhk@gnu.ac.kr

Abstract: - Computational analysis has been performed for unsteady fluid flow in transonic regime over rocket like configurations. Finite volume based numerical method has been used and k-ω SST based turbulence model is applied. The purpose of this work is to analyze the unsteady aerodynamic character of the flow and establish the validity and accuracy of the computational process. The validation has been done by comparing the RMS(root mean square) value of the computed instantaneous pressure at different time step against the experimental results. Apart from this, the PSD (Power Spectral Density) values for the pressure fluctuation are also calculated and compared with experiment. The effects of Mach number and geometry configuration on the location of the shockwave have also been considered and comparison results are presented in detail.

Key Words : k-ω SST, DES, Transonic Flow, Rocket Configuration

1. Introduction

Aerodynamic character of unsteady transonic flow over two different type of launch vehicle nose has been analysed in this work.A finite volume based solver is used for the computation pocess.It is well known fact that the fluid-resistence experienced by the launch vehicle/missile during its flight is highly dependent on the shape of its nose and the mach number of the flight. So far, too many experiments has been done on different nose shape.In this presentation, we try to seek whether we can understand the flow characteristics by means of computation and we try to compare the data achieved from these computational works with that of available experiment result.

Application of Computational Fluid Dynamics (CFD) for flow over launch vehicles is a well-accepted style of analysis. In 1996 Azevedo *et. al.*[3] used a finite volume solver on segregated grid with central-difference scheme to analyze flow over launch vehicle.In 1998 F. Grasso *et. al.*[4] used turbulence model with finite volume based code for flow over missile body.Mehta[5] (2001) has applied the FVM based code for transnic flow over launch vehicle.

In this work presented here, we tried to apply the turbulence models developed in the field of CFD to analyze transonic flow over the launch vehicle nose.The purpose is to show and establish the fact that we can have the understanding of unsteady aerodynamics with the help of the computational work .Afterwards, we try to discuss our result with slender body theory for the location and movement of shock.

2. Computational Background

In the present work, the analysis is done for two different geometry from the NASA report[1].The detailed description is given in Table 1 & Figure 1.

Table 1. Details of considered geometries & cases

Model No	Mach Number	Nose Type
IV	0.79 0.91	Ellipsoidal, Fineness ratio=2
V	0.788 0.95	Hemisphere-cone-cylinder

The flow condition for the computation is derived from the NASA report[2] and Reynolds Number (Re)

is kept same as the experiment. The mesh size is maintained properly as per implemented turbulence models (k-ω sst, Detached Eddy Simulation).The result of the work shows good agreement with the experimental data.The objective of this analysis is to understand the unsteady aerodynamic characteristic of the flow corresponding payload distribution reflected by the pressure fluctuation over the gemetry.

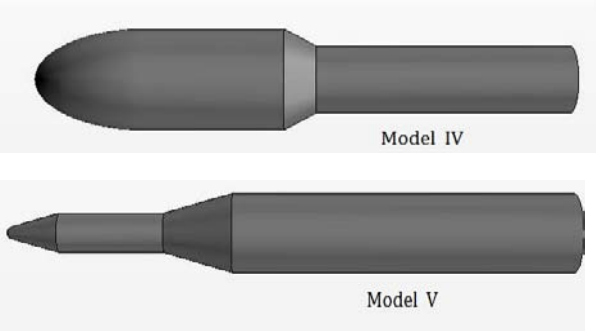

Fig. 1 Geometric configurations for rocket models

2.1 Governing Equations and Boundary Conditions

We Solve the governing equation for compressible flow given in Eqs.(1)-(3).

$$\frac{\partial \rho}{\partial t} + \frac{\partial}{\partial x_i}(\rho u_i) = 0 \quad (1)$$

$$\frac{\partial}{\partial t}(\rho u_j) + \frac{\partial}{\partial x_i}(\rho u_i u_j + p\delta_{ij} - \tau_{ij}) = \rho f_i \quad (2)$$

$$\frac{\partial}{\partial t}(\rho E) + \frac{\partial}{\partial x_i}\left[\rho u_i\left(E + \frac{p}{\rho}\right) - \tau_{ij}u_j + q_i\right] = \rho f_i u_i \quad (3)$$

where ρ is the density of fluid,*t* is the time, x_i and u_i (i=1,2,3) represents the three components of cartesian co-ordinate system, respectively and velocity,δ_{ij} is the croneker delta function,p is the variable representing the pressure, E=[e+($\vec{u}$•$\vec{u}$)/2] is the total specific energy , q_i is the tensor form of heat flux, f_i is the accelaration of gas due external force (e.g. gravitation, electromagnetic force etc) and τ_{ij} is the stress tensor.

Some assumptions are made to solve the set of governing equations:-

- Newtonian fluid flow which enables equation (4) for calculation of the stress tensor.

$$\tau_{ij} = 2\mu S_{ij} \quad (4)$$

where $S_{ij} = \frac{1}{2}\left(\frac{\partial u_i}{\partial x_j} + \frac{\partial u_j}{\partial x_i}\right) - \frac{1}{3}\frac{\partial u_k}{\partial x_k}\delta_{ij}$

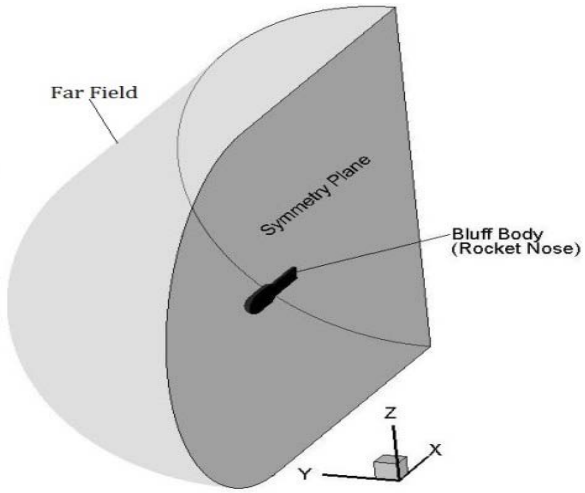

(a) Model IV

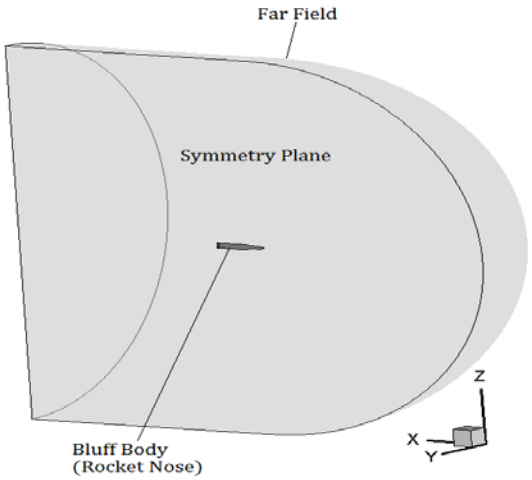

(b) Model V

Fig. 2 Computational domains

- Ideal gas flow which enables equation (5) for calculation of density.

$$\rho = \frac{p}{RT} \quad (5)$$

where

p = Opertating pressure + gauge pressure

- Availability of Fourier's law [equation (6)] of heat tranfer to calculate the heat flux.

$$q_j = \lambda \frac{\partial T}{\partial x_j} \quad (6)$$

λ is the thermal conductivity

Figure 2 shows the computationl domain for the analysis where positive direction of X-axis represents the flow direction. The "Far Field" boundary condition (BC) is applied by keeping the mach number fixed.Thus, the total pressure is computed as $p_{total} = p_{static}(1 + \frac{\gamma-1}{2}M^2)^{\gamma/(\gamma-1)}$. No-slip wall condition is applied on the bluff body

and a symmetry plane is defined to reduce the required number of mesh.

2.2 Finite Volume Descretization

The integral form of Eqs.(1)-(3) can be described in vector form as given in Eqs.(7)-(9).

$$\frac{d}{dt}\int_{CV}\rho dV = -\oint_{CS}\rho\vec{u}\bullet\vec{n}dA \quad (7)$$

$$\frac{d}{dt}\int_{CV}\rho\vec{u}dV + \oint_{CS}\rho\vec{u}\vec{u}\bullet\vec{n}dA = -\oint_{CS}p\vec{\vec{I}}\bullet\vec{n}dA + \oint_{CS}\vec{\vec{\tau}}\bullet\vec{n}dA \quad (8)$$

$$\frac{d}{dt}\int_{CV}\rho EdV + \oint_{CS}\rho E\vec{u}\bullet\vec{n}dA = -\oint_{CS}p\vec{u}\bullet\vec{n}dA + \oint_{CS}\vec{\vec{\tau}}\bullet\overrightarrow{u}\bullet\vec{n}dA \quad (9)$$

where V and A are used to represent volume and area of the computational cell.The term CV stands for the control volume and CS is for control surface which is in fact the boundary of the CV. Lastly, $\vec{n}$ is the normal vector to the surface of the computational cell.

We use the integral representation to explain the FVM descretization of the Navier-Stokes eqn.The semi-discretized form of the governing equations considering eulerian time step for a point P can be presented as:-

$$V_p\left(\frac{\rho^{n+1}-\rho^n}{\Delta t}\right)_P = -\sum_f\left(\rho\overrightarrow{u_f}\bullet\overrightarrow{S_f}\right) \quad (10)$$

$$V_p\left[\frac{(\rho u_i)^{n+1}-(\rho u_i)^n}{\Delta t}\right]_P + \sum_f\rho(\overrightarrow{u_f}\bullet\overrightarrow{S_f})u_{i,f} = -\sum_f P_f^{n+1}\bullet S_{i,f} + \sum_f\gamma(\nabla u_i)_f\bullet S_f \quad (11)$$

$$V_p\left[\frac{(\rho E)^{n+1}-(\rho E)^n}{\Delta t}\right]_P + \sum_f\rho(\overrightarrow{u_f}\bullet\overrightarrow{S_f})E_f = -\sum_f P_f^{n+1}\left(u_f\bullet S_{if}\right) + \sum_f\gamma(\nabla u_i)_f\bullet S_f \quad (12)$$

The index $n+1$ and n stands for n-th time step u_f represents the value of velocity in the direction of face normal vector $\vec{n}$, V_p is the volume of the computational cell.Also, S_{if} is the *i*-th component of $\overrightarrow{S_f}$.

It should be noted that, the temporal discretization used in this presentation is a eulerian time step.For computation of unsteady flow, we need to use a higher order temporal discretization (e.g Runge Kutta) in our analysis.

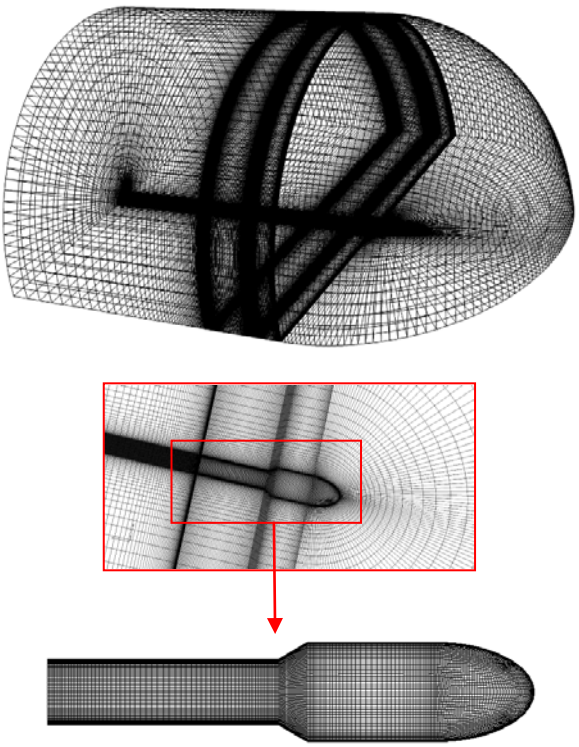

(a) Model IV

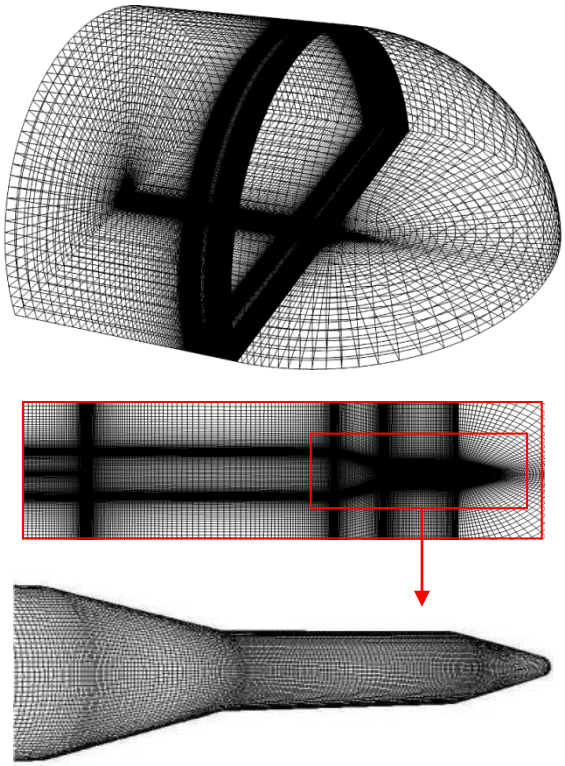

(b) Model V

Fig. 3 Computational mesh

2.3 Computational mesh and numerical solver

A body-fitted, cartesian type, computational mesh has been prepared for each domain considered for this analysis. Highly fine quality of grid has been maintained near the wall body to assure 1< y+

<5.The hexahedral grid size is stretched at far field direction, such that the boundaries of the domain has a coarse surface mesh.

The solver used for the simulation is a finite volume type numerical package (ANSYS FLUENT).The applied density based numerical scheme for the analysis is a implicit second order accurate one in space and time. For the temporal discretization, two step Runge-kutta algorithm has been applied.For each case, prior to the unsteady simulation, a steady state solution of the flow field is used for initialization purpose. The time step was chosen to be of 10^{-5}, to catch the unsteady flow structures properly.The numerical discretization of the governing equation has already been described in previously.In this section, we'll try to focus on the turbulence scheme.The choice of turbulence scheme depends on the issue of capturing the instabilities of the flow physics and associated time-history effects (e.g convection and diffusion of tubulent energy).Obviously the k-ω family of turbulence models is a natural choice for this.The next step is to select a appropriate candidate among the different form of k-ω model.Menter's k-ω SST model[6] surpasses all other candidates in the list since it dominates over the limitations of original k-ω & BSL k-ω[6] in production of highly accurate boundary layer solution due to its modified near wall treatment.Apart from the k-ω SST model, a DES(Detatched Eddy Simulation) model has also been applied for one set of simulation.Brief descriptions of the turbulence models with associated equations are described here. The k-ω SST, a modified form of orginal k-ω model by Wilcox[7], uses twon extra governing equations to account for the turbulence in flow.As shown in proper conservation form, one equation is for turbulence kinetic energy k (Eq.13) while other is for specific dissipation ω (Eq.14).

$$\frac{\partial(\rho k)}{\partial t}+\frac{\partial\left(\rho u_j k\right)}{\partial x_j}= P-\beta^*\rho\omega k+\frac{\partial}{\partial x_j}\left[(\mu+\sigma_k\mu_t)\frac{\partial k}{\partial x_j}\right] \quad (13)$$

$$\frac{\partial(\rho\omega)}{\partial t}+\frac{\partial(\rho u_j\omega)}{\partial x_j}= P+\frac{\partial}{\partial x_j}\left[(\mu+\sigma_\omega\mu_t)\frac{\partial\omega}{\partial x_j}\right]+\alpha \quad (14)$$

The associated constants are calculated as given in Eqn set (15)

$$\begin{aligned}
\alpha &= 2(1-F_1)\frac{\rho\sigma_{\omega 2}}{\omega}\frac{\partial k}{\partial x_j}\frac{\partial k}{\partial x_j}\\
P &= \tau_{ij}\frac{\partial u_i}{\partial x_j}\\
\tau_{ij} &= \mu_t\left(2S_{ij}-\frac{2}{3}\frac{\partial u_k}{\partial x_k}\delta_{ij}\right)-\frac{2}{3}\rho k\delta_{ij}\\
u_t &= \frac{\rho a_1 k}{\max\left(a_1\omega,\Omega F_2\right)}\\
S_{ij} &= \frac{1}{2}\left(\frac{\partial u_i}{\partial x_j}+\frac{\partial u_j}{\partial x_i}\right)
\end{aligned} \quad (15)$$

In the given equations a_1, $\sigma_{\omega 2}$, σ_ω etc are equation constants. The numerical solver calculates the dissipation term (Y_k) of the turbulent kinetic energy as expressed in Eq.(16).

$$Y_k=\rho\beta^* f_{\beta^*}k\omega \quad (16)$$

where β^* is a equation constant.

In Menter's k-ω SST model the term f_{β^*} is treated as a constant with the value of unity for most cases.However in DES model it is calculated as shown in Eq.(17).

$$f_{\beta^*}=max\left[\left({}^{L_t}/_{C_{DES}\Delta}\right),1\right] \quad (17)$$

where L_t is the turbulent length scale, C_{DES} is the calibration constant in DES and Δ is the maximum grid spacing. This is the fundamental difference between DES and k-ω SST numerical schemes.

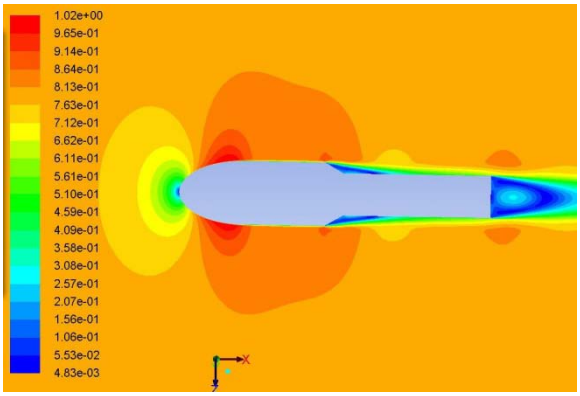

(a) Model IV, M=0.79, AoA=0, t=0.5 sec

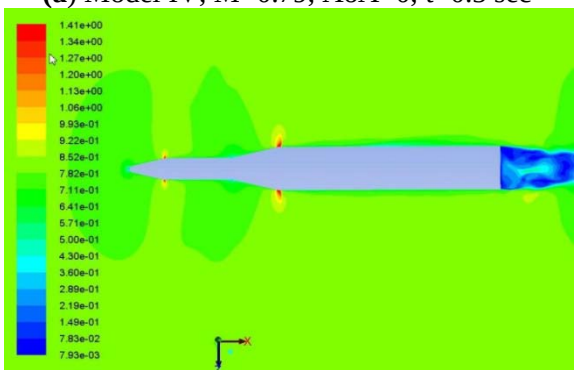

(b) M=0.788, AoA=0, t=0.5 sec

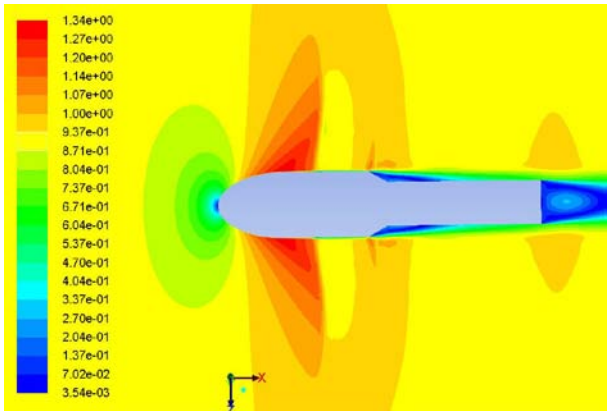

(c) Model IV, M=0.91, AoA=0, t=0.5s

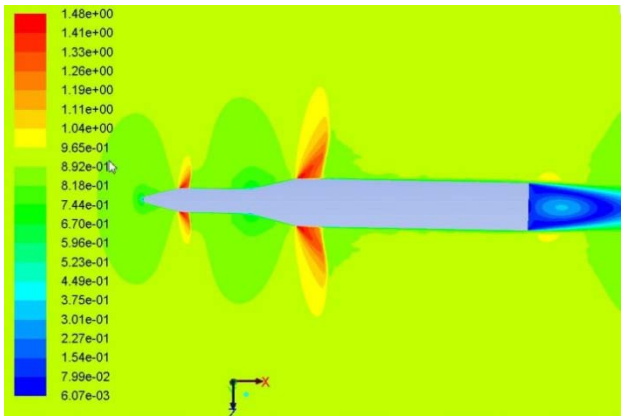

(d) Model V, M=0.95, AoA=0, t=0.5 sec

Fig 4. Instantaneous Mach contours (Model V).

3. Results and Discussion

Figure 4 shows the instantaneous mach contour at t=0.5s in a streamwise cross secion for different mach number and geometries. The localized high value of mac number represents the occurance of shockwaves. As we can see the development of "mach cone" is more prominent with increasing Mach number of the flow. During low mach number, the instabilities are more effective as shown in Fig.4(c) due to lower inertia force which can't dominate the viscous force totally. Same character of the unsteady flow can be obtained from the intantaneous static pressure contour as presented in Fig.5. The appearance of vortex rings at shock are given in Figure 6 .

The validation process of current computation is done by comparing the root mean square (RMS) value of the coefficient of instantaneous Pressure. The value of the pressure coefficient (Cp) obtained by Eq.(18) where P_{static} is the static pressure, P_{ref} is the free stream pressure, v_{ref} is the free stream velocity and ρ_{ref} is the free stream density of the fluid.

$$C_p = \frac{(P_{static} - P_{ref})}{\frac{1}{2}\rho_{ref}(v_{ref})^2} \quad (18)$$

The instantaneous solution has been saved for each time. step.The $(\Delta C_p)_{instantaneous}$ for a particular time step can be calculated as defined in Eq.(19) where $(C_p)_{instantaneous}$ is the pressure coefficient calculated for a particular time step from the instantaneous solutions and $(C_p)_{steady}$ is the same calculated for steady flow.

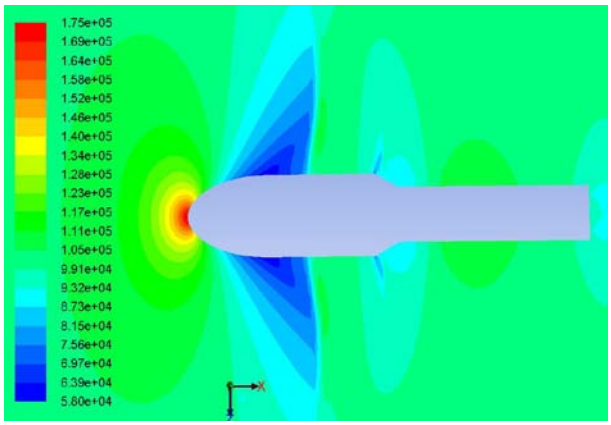

(a) Model IV, M=0.91, AoA=0, t=0.5 sec

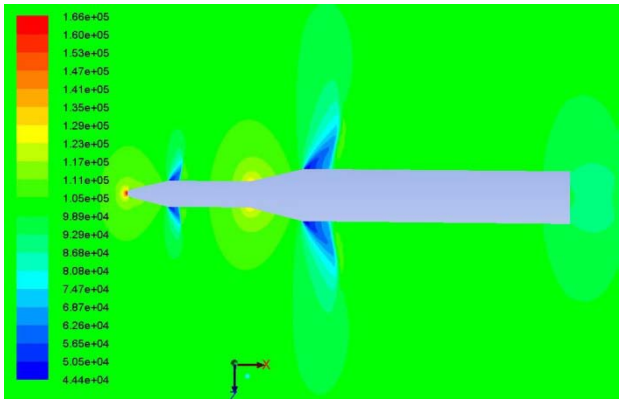

(b) Model V, M=0.95, AoA=0, t=0.5 sec

Fig 5. Instantaneous static pressure contours.

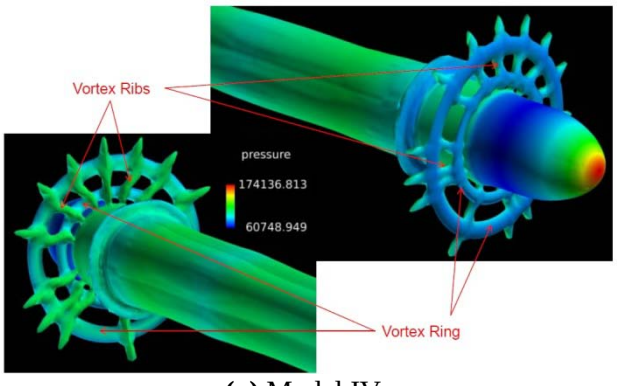

(a) Model IV

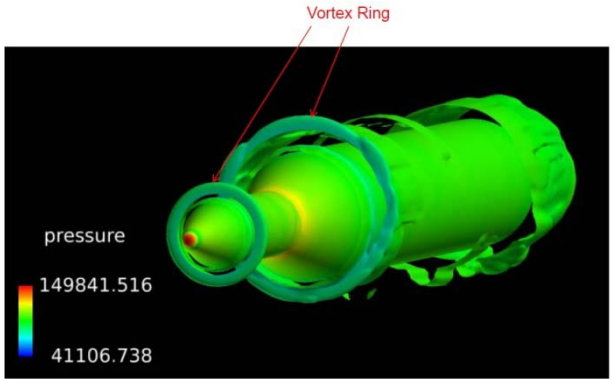

(b) Model V

Fig. 6 Vortex ring and total pressure plots

Afterwards the RMS value of the differenc of unsteady pressure coefficient is calculated as shown in equation (20).

$$\left(\Delta C_p\right)_{instantaneous} = \left(C_p\right)_{steady} - \left(C_p\right)_{instantaneous} \quad (19)$$

$$\left(\Delta C_p\right)_{RMS} = \left[\sum_n \frac{\left\{\left(\Delta C_p\right)_{instantaneous}\right\}^2}{n}\right]^{1/2} \quad (20)$$

Figure 7 represents the comparison of calculated $\left(\Delta C_p\right)_{RMS}$ with available results[1]. "x" is the streamwise distance from nose and "D" is the maximum diameter of the geometry. High peaks in $\left(\Delta C_p\right)_{RMS}$ represents the shockwaves location.

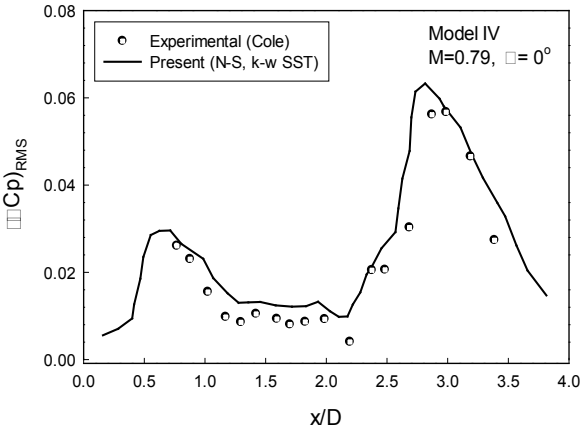

(a) Model IV (M=0.79)

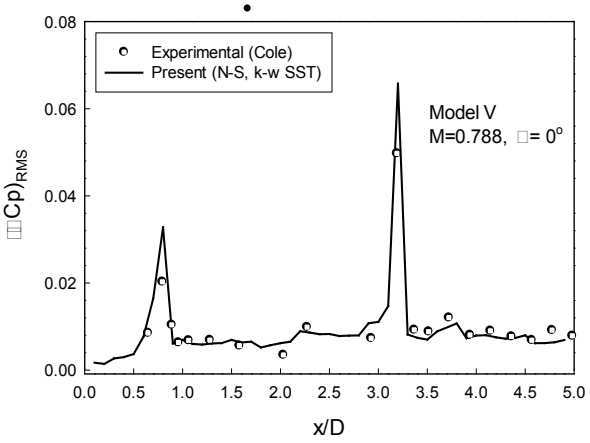

(b) M=0.788

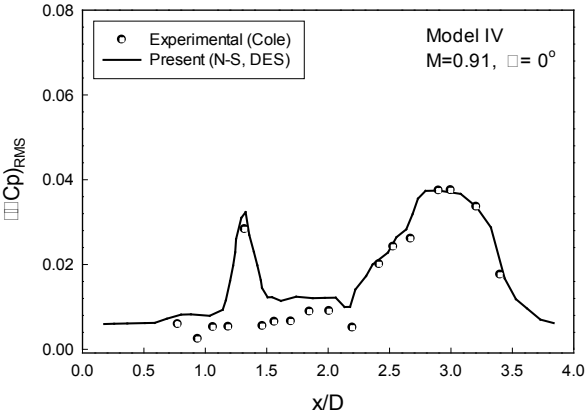

(c) Model IV (M=0.91)

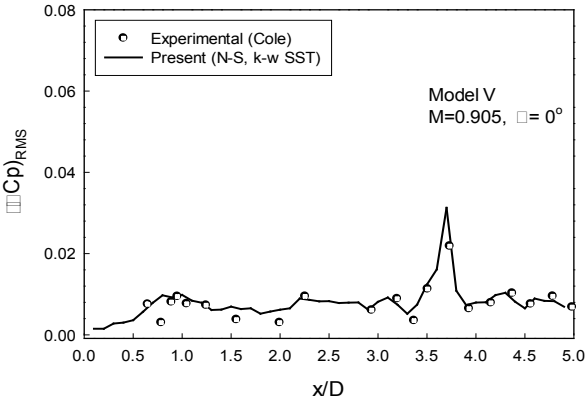

(d) Model V (M=0.905)

Fig. 7 Comparison of the calculated RMS value of ΔCp with experiment

Figure 8 gives another validation from the frequency domain analysis in terms of the power spectral density (PSD) of the instantaneous pressure computed and saved at each time step. The PSD of any signal x(t) ,as per its mathematical definition goes, is the Fourier transform of the autocorrelation function of x(t).The Fourier transform of the autocorrelation sequence of a signal x(t) as the can expressed by equation (21) and the PSD is expressed

by equation (22).Furthermore, equation (23) gives the averaged PSD frequency.

$$F(f) = \sum_{t=1}^{N} x(t) e^{-i2\pi ft} \quad (21)$$

$$P_{xx}^{i}(f) = \frac{1}{\sum_{t=1}^{N} (w(t))^2} \left[\sum_{n-1}^{N} x_i(t) w(t) e^{-i2\pi ft} \right]^2 \quad (22)$$

$$f_{avg} = \frac{\sum_{i=1}^{L} P_{xx}^{i} f^{i}}{\sum_{i}^{L} P_{xx}^{i}} \quad (23)$$

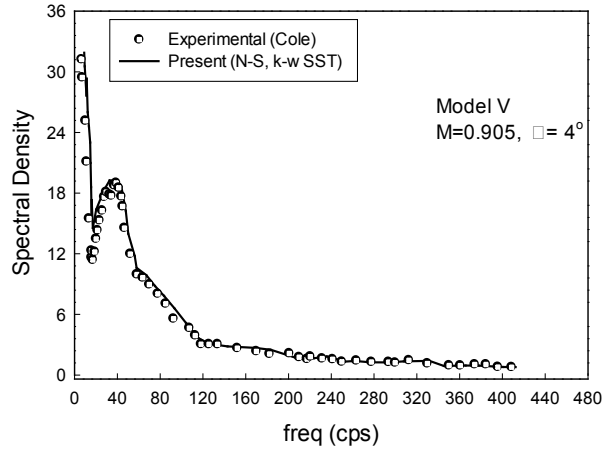

Fig. 8 Comparison of calculated power spectral density with the experiment for the Model V at x/D=0.907 and M=0.905.

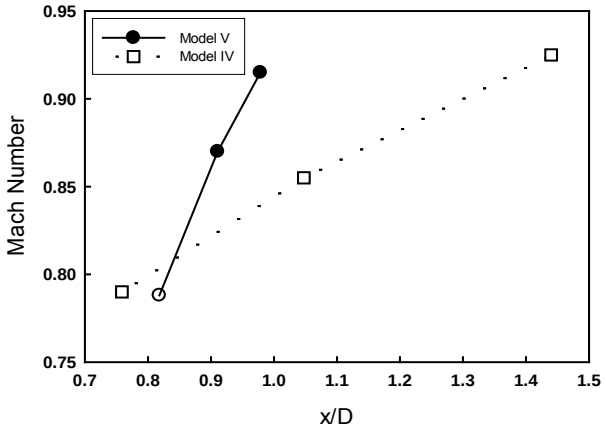

Fig. 9 Comparison of the first shock wave position for different Mach numbers

The pressure fluctuations in the computed results reflect the possible unsteady bending load on the rocket nose geometry.The results of the analysis has shown that these unsteady bending loads on a vehicle with a cylindrical body are small if the nose is sufficiently slender. Obviously the higher rate of area reduction affects the location and amplitude of the shockwave. The effect of Mach number on the first shock's location is presented in Fig. 9. It is shown in this study that the location of the shock wave positon can be sensitively varied depending on both Mach number and the shape of the rocket nose configuration.

3. Conclusion

In this study, unsteady aerodynamic analysis for different rocket configurations have been conducted using computational fluid dynamics technique. Numerical process for the calculation of unsteady pressure coefficient is also suggested in detail. The present numerical results based on k-ω SST turbulent model shows very good agreement with the previous experimental data. It is also shown in this study that the location of the shock wave positon can be sensitively varied depending on both Mach number and the shape of the rocket nose configuration.

Acknowledgement

This work was performed with the support of the National Research Foundation of Korea (NRF) funded part of the business development of space launch vehicles.

References

(1) Charles F. Coe, " The Effect of Some Variations in Launch-Vehicle Nose Shape on Steady and Fluctuating Pressures at Transonic Speeds", *NASA TM X-646*, March 1962.

(2) "Characteristics of Six Research Wind Tunnels of the Ames aeronautical Lab", *Washington*, 1957.

(3) Azevedo J. L. F, Moraes Jr. P, Maliska C. R, Marchi C. H, and Silva A. F. C. "Code validation for high-speed flow simulation over satellite launch vehicle" *Journal of Spacecraft and Rockets*, Vol. 33, No 1, pp 15–21, 1996

(4) F. Grasso and G. Iaccarino, “Influence of Crossflow and Turbulence on the Vortex Flow Around a Supersonic Missile,” Journal of Spacecraft and Rockets, Vol. 35, No. 1, pp. 37-45, 1998

(5) Mehta R. C. "Comparative study of surface pressure fluctuations over bulbous heat shields at Mach number=0.95", Computers and Fluids vol. 30 issue 6 July, 2001. p. 689-709

(6) Menter, F. R., "Two-Equation Eddy-Viscosity

Turbulence Models for Engineering Applications," AIAA Journal, Vol. 32, No. 8, August 1994, pp. 1598-1605

(7) Wilcox, D. C., "Formulation of the k-omega Turbulence Model Revisited," AIAA Journal, Vol. 46, No. 11, 2008, pp. 2823-2838.

(8) White, F. M., "Viscous Fluid Flow" McGraw-Hill, New York, 1974